ESAIM: PROCEEDINGS, December 2012, Vol. 38, p. 298-318
F. Coquel, M. Gutnic, P. Helluy, F. Lagoutière, C. Rohde, N. Seguin, Editors

EVALUATION OF INTERFACE MODELS FOR 3D-1D COUPLING OF COMPRESSIBLE EULER METHODS FOR THE APPLICATION ON CAVITATING FLOWS

Martina Deininger[1], Jonathan Jung[2], Romuald Skoda[3], Philippe Helluy[2] and Claus-Dieter Munz[4]

Abstract. Numerical simulations of complete hydraulic systems (e.g. diesel injectors) can, due to high computational costs, currently not be done entirely in three dimensions. Our aim is to substitute the 3D solver by a corresponding 1D method in some parts of the system and develop a solver coupling with suitable interface models. Firstly, we investigate an interface model for non-cavitating flow passing the interface. A flux-coupling with a thin interface approach is considered and the jump in dimensions at the interface is transferred to an additional variable ϕ, which switches between the 3D and the 1D domain. As shown in two testcases, the error introduced in the vicinity of the interface is quite small. Two numerical flux formulations for the flux over the 3D-1D interface are compared and the Roe-type flux formulation is recommended. Secondly, extending the first method to cavitating flows passing the interface, we divide the density equation in two equations - one for liquid and one for vapor phase of the two-phase fluid - and couple the two equations by source terms depending on the free enthalpy. We propose two interface models for coupling 3D and 1D compressible density-based Euler methods that have potential for considering the entire (non-) cavitating hydraulic system behaviour by a 1D method in combination with an embedded detailed 3D simulation at much lower computational costs than the pure 3D simulation.

1. Introduction

For the simulation of cavitating fluid flow (liquid and vapor) in complex hydraulic systems (e.g. diesel injectors) a compressible density-based three dimensional Euler model is used. A consideration of the entire flow path in a hydraulic system is currently not possible by the 3D solver due to high computational costs. To reach acceptable computation time commonly the complete hydraulic system is simulated in one dimension and time averaged boundary conditions for a 3D method is achieved at predefined locations. This 3D solver is additionally applied for interesting, e.g. cavitating, parts of the system, using the time averaged boundary conditions given by the 1D solver. Instead of performing this weak coupling of 3D and 1D methods, an interface model for a strong 3D-1D solver coupling is developed, coupling at each Runge-Kutta stage (four times each time step) and representing the bidirectional interaction of system hydraulics and three dimensional cavitating flow (liquid and vapor). Generally, to couple a pressure-based 3D solver using the Rayleigh Plesset cavitation

[1] Robert Bosch GmbH, Wernerstraße 51, 70469 Stuttgart-Feuerbach, e-mail: Martina.Deininger@de.bosch.com
[2] University of Strasbourg, 7 rue René Descartes, 67000 Strasbourg, e-mail: jonathan.jung@unistra.fr
[3] Ruhr University Bochum, Universitätstr. 150, 44801 Bochum
[4] University of Stuttgart, Pfaffenwaldring 21, 70569 Stuttgart

Article published online by EDP Sciences and available at http://www.esaim-proc.org or http://dx.doi.org/10.1051/proc/201238016

model and a 1D solver, it is sufficient to exchange pressure p and velocity u (or volume flow Q) at the boundaries between the 3D and 1D solver (compare e.g. [NII2011]). This coupling strategy is not sufficient for compressible density-based solvers using homogeneous density cavitation model. Instead of pressure p and velocity u, we use numerical fluxes to couple 3D and 1D density-based Euler methods and achieve two coupling algorithms. The first considered model is valid for non-cavitating flows passing the interface. This interface model is based on [HH2007] and is described in section 2. Secondly, in section 3, we consider cavitation bubbles passing the interface (compare [CCJK2006]). We emphasize that for both models cavitation is allowed to occur inside the 3D domain.

To simulate three dimensional cavitating fluid flow the compressible density-based 3D-CFD code Catum (CAvitation Technical University of Munich, [SSST2008]) is utilized. Catum solves the 3D Euler equations

$$\partial_t W + \partial_x F_{3D}(W) + \partial_y G_{3D}(W) + \partial_z H_{3D}(W) = 0, \tag{1.1}$$

where

$$\begin{aligned} W &= (\rho, \rho u, \rho v, \rho w)^T, & (1.2)\\ F_{3D}(W) &= (\rho u, \rho u^2 + p(\rho, T_0), \rho uv, \rho uw)^T, & (1.3)\\ G_{3D}(W) &= (\rho v, \rho uv, \rho v^2 + p(\rho, T_0), \rho vw)^T, \\ H_{3D}(W) &= (\rho w, \rho uw, \rho vw, \rho w^2 + p(\rho, T_0))^T, \end{aligned}$$

with the velocities $u(x, y, z, t) = u$, $v(x, y, z, t) = v$, $w(x, y, z, t) = w$ in x-, y-, z-direction, and time t, using a finite volume scheme with a MUSCL reconstruction scheme and an explicit Runge-Kutta 4-stage scheme which yields second order in space and time. For detail of the numerical flux formulation of Catum and the scheme see section 2.3.1 or [SSST2008]. The energy equation is neglected which results in the assumption of isentropic flow and a barotropic equation of state $p(x, y, z, t) = p(\rho, T_0) = p$ (p pressure, ρ density, T_0 fixed initial temperature). Neglecting the energy equation is not realistic, but a good approach using the available measured fluid data. As a consequence we obtain an isentropic equilibrium model which is equivalent to the assumption that vaporization and condensation occur infinitely fast. As fluid, we use a measured test-fluid, which behaves like diesel. Its pressure law is determined not by a formula but by a table including the pressure p and the homogeneous density $\rho = \alpha\rho_{liq} + (1 - \alpha)\rho_{vap}$ with the liquid ρ_{liq} and vapor density ρ_{vap}, α volume fraction of the liquid phase and the speed of sound c, leading to hyperbolic equations. Especially the split densities ρ_{liq} and ρ_{vap} are essentially needed for the "cavitating" interface model (see section 3). The Riemann-like flux formulation of Catum has been successfully applied for the computation of cavitating flow fields and for the evaluation of cavitation erosion (see [SIMMSA2011]).

Besides the 3D version of Catum, we have available a 1D version of the code, which solves the one dimensional Euler equations

$$\partial_t W + \partial_x F_{1D}(W) = 0, \tag{1.4}$$

with $W = (\rho, \rho u)^T$ and $F_{1D}(W) = (\rho u, \rho u^2 + p(\rho, T_0))^T$ and the same barotropic equation of state $p(\rho, T_0)$ as for the three dimensional Euler equations (1.1). The EOS is given such that system (1.1) and (1.4) are hyperbolic.

An exemplary mesh for a 3D-1D coupling is depicted in Figure 1.1. The coupling interface between 3D and 1D domain is located at $x_{IF} = 0$. Consequently, the 3D-mesh and thus the 3D-solver is located at $x < 0$ and the 1D part at $x > 0$. Both domains have the same cross-section in y- and z-direction with no jump in geometry at the coupling interface. The interface connected cells in the 3D part are defined by

$$i = 0, \quad j = 1, \ldots, N_y, \quad k = 1, \ldots, N_z \tag{1.5}$$

with number of cells $N_y = N_z =: N$ for simplicity.

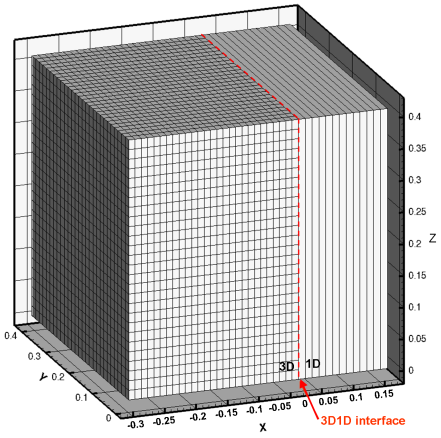

FIGURE 1.1. Geometry for the 3D-1D coupling, with the 3D mesh on the left and the 1D mesh on the right side of the 3D-1D interface located at $x_{IF} = 0$.

2. INTERFACE MODEL FOR NON-CAVITATING FLOWS

Obviously, a three-dimensional code (based on a three dimensional system) applied on a "one-dimensional" domain does not behave as a one-dimensional code (based on a one-dimensional system) on the same domain. We want to look for a condition for a three-dimensional code to behave as a one-dimensional code.

2.1. **A necessary and sufficient coupling boundary condition**

We use the 3D-1D discretization depicted in Figure 1.1 with the interface at $x_{IF} = 0$, the cells on the left of interface are referenced by formula (1.5). We assume that the domain $\{x \geq 0\}$ is discretized as one dimensional domain by a row of hexahedral cells with volume $\Delta x \times (\Delta y =: L) \times (\Delta z =: h)$, the cells are referenced by indexes i for $i \geq 1$ (the cell $i = 1$ touches the interface $x_{IF} = 0$ (see Figure 2.1)). The surfaces of cell i are distinguished by the compass-like notation E_i (east), W_i (west), N_i (north), S_i (south), U_i (upper), L_i (lower) as depicted in Figure 2.1.

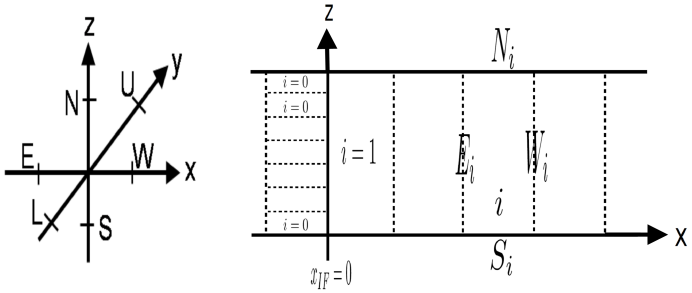

FIGURE 2.1. Compass notation for surfaces of hexahedral cells in the 1D domain $x > 0$.

As the domain $\{x \geq 0\}$ is a one dimensional domain, we assume that at any time t_n, the cross velocity satisfy

$$\forall i \geq 1,\ v_i^n = w_i^n = 0.$$

We want to deduce a condition which ensures $\forall i \geq 1,\ v_i^{n+1} = w_i^{n+1} = 0$ at time $t_{n+1} = t_n + \Delta t$ for $x \geq 0$. Applying a three dimensional Godunov scheme $(\cdot)^{God}$ (see [G1959]) on the third equation of (1.1) on domain $\{x > 0\}$ (one-dimensional domain), gives

$$\begin{aligned} hL\Delta x[(\rho v)_i^{n+1} - (\rho v)_i^n] \quad &+ \quad h\Delta x\Delta t[(\rho v^2 + p)_{N_i}^{God} - (\rho v^2 + p)_{S_i}^{God}] \\ +hL\Delta t[(\rho uv)_{E_i}^{God} - (\rho uv)_{W_i}^{God}] \quad &+ \quad L\Delta x\Delta t[(\rho vw)_{U_i}^{God} - (\rho vw)_{L_i}^{God}] = 0. \end{aligned} \tag{2.1}$$

Using the wall condition (see [BGH2000]) as boundary condition for N_i (resp. S_i) and defining $\overrightarrow{N_{N_i}}$ (resp. $\overrightarrow{N_{S_i}}$) as the unit outward normal vector on the north surface N_i (resp. the south surface S_i), the pressure satisfies:

$$p_{N_i}^{God} = p^{God}(W_i^n, \widehat{W_{N_i}^n}, \overrightarrow{N_{N_i}}),\ \ p_{S_i}^{God} = p^{God}(W_i^n, \widehat{W_{S_i}^n}, \overrightarrow{N_{S_i}}),$$

where $\widehat{W_{N_i}^n} = \widehat{W_{S_i}^n} = \widehat{W_i^n} = (\rho_i^n, (\rho u)_i^n, -(\rho v)_i^n, (\rho w)_i^n)$ stands for the mirror state of W_i^n. As it holds $v_i^n = 0$ for $x > 0$, we obtain $\widehat{W_i^n} = W_i^n$, giving

$$v_{N_i}^{God} = v_i^n = v_{S_i}^{God} = 0,\ \ p_{N_i}^{God} = p_i^n = p_{S_i}^{God},\ \ \rho_{Ni}^{God} = \rho_i^n = \rho_{S_i}^{God}, \tag{2.2}$$

with the barotropic equation of state $p(\rho, T_0)$. Inserting equation (2.2) to equation (2.1) the second term is cancelled. With a similar argument for surfaces U_i and L_i, we obtain that $(\rho vw)_{U_i}^{God} = (\rho vw)_{L_i}^{God} = 0$ and $v_{W_i}^{God} = 0$. Altogether inserted in equation (2.1), yields

$$hL\Delta x(\rho v)_i^{n+1} + hL\Delta t(\rho uv)_{E_i}^{God} = 0. \tag{2.3}$$

In domain $x > \Delta x$, $v_{E_i}^{God} = 0$ holds. Assuming no vacuum (i.e. $\rho_i^{n+1} > 0$), equation (2.3) provides $v_i^{n+1} = 0$ for all cells in $x > \Delta x$ (i.e. $i \geq 2$).

For the cell that touches the interface (i.e. $i = 1$), we obtain a condition for the third component of the numerical fluxes at the interface ($x_{IF} = 0$) denoted by surface $E_{i=1}$:

$$v_{i=1}^{n+1} = 0 \Leftrightarrow (\rho uv)_{E_{i=1}}^{God} = 0. \tag{2.4}$$

The coupling condition can be written as

$$\forall i \geq 1,\ v_i^{n+1} = 0 \Leftrightarrow (\rho uv)_{E_{i=1}}^{God} = 0. \tag{2.5}$$

Further applying the Godunov scheme on the fourth equation of (1.1) gives an equation for the momentum ρw analog to (2.3). Using the same arguments as for equation (2.3), we obtain the condition:

$$\forall i \geq 1,\ w_i^{n+1} = 0 \Leftrightarrow (\rho uw)_{E_{i=1}}^{God} = 0. \tag{2.6}$$

Notation 1. (Interface: $+,-$) *Commonly, for the left and the right side of a cell interface the indices 'L' and 'R' are used. For general problems, we use this notation. But to denote the coupling interface connected problems, we define '$-$' for the left and '$+$' for the right side of the interface located at $x_{IF} = 0$ (compare Figure 2.2, right).*

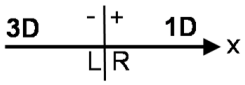

FIGURE 2.2. The left side of the interface $x < x_{IF} = 0$ is denoted by '$-$' and the 3D equations (1.1) are applied. Analog the right side of the interface $x > x_{IF} = 0$ is denoted by '$+$' and the 1D equations (1.4) are applied.

The equations (2.5) and (2.6) are the wanted necessary and sufficient coupling boundary conditions to fit to pure one-dimensional simulation in the right domain. The condition depends only on the value of the ρv- and the ρw- components of the 3D-solver numerical flux at the interface $x = 0^+$.

Definition 2. (admissible coupling boundary) *A 3D-1D coupling boundary is defined as admissible, if the ρv- and the ρw- components of the 3D-solver numerical flux at the interface $x = 0^+$ are zero:*

$$\begin{cases} (\rho uv)^+ = 0, \\ (\rho uw)^+ = 0. \end{cases} \tag{2.7}$$

A necessary and sufficient condition for the 3D solver to give a consistent one dimensional numerical flux at the coupling boundary is deduced. To switch at $x_{IF} = 0$ from the $N \times N$ numerical fluxes $F_{3D}(W) := (\rho u, \rho u^2 + P, \rho uv, \rho uw)^T$ (defined in (1.3)) in x-direction at the left side (3D domain) of the interface to one numerical flux $F_{1D}(W) := (\rho u, \rho u^2 + P)^T$ (see (1.4)) at the right side (1D domain) of the interface, we want to define a flux F_{IF} in the x-direction at the interface $x_{IF} = 0$ satisfying the coupling condition (2.7).

2.2. **A conservative admissible interface model**

Based on the admissible coupling boundary (Definition 2) we develop a conservative admissible interface model. An a priori obvious candidate as a 3D-1D coupling interface model immediately arises considering the projection of the three dimensional Euler equations (1.1) on the plane (O, y, z). We obtain

$$\partial_t W + \partial_x F_{IF}(W) \quad = \quad 0, \tag{2.8}$$

with $W = (\rho, \rho u, \rho v, \rho w)$ and $F_{IF}(W) = F_{3D}(W) = (\rho u, \rho u^2 + p, \rho uv, \rho uw)$ defined by equations (1.2) and (1.3). The interface model (2.8) does not respect the coupling condition (2.7) and the cross-velocities v and w will not remain zero in the 1D domain as expected (see [HH2007]).

To achieve an admissible interface model, we distinguish the three and one dimensional domain with the function

$$\phi(x, y, z, t) \quad := \quad \begin{cases} 1\,, & x < 0, \\ 0\,, & x > 0, \end{cases} \tag{2.9}$$

which does not depend on time t and vanishes for the 1D domain assumed for $x > 0$ and we insert ϕ to equation (2.8). We receive the admissible interface model

$$\partial_t Y + \partial_x F_{IF}(Y) = 0, \tag{2.10}$$

with the vector of conservative variables $Y := (\phi, W^T)^T = (\phi, \rho, \rho u, \rho v, \rho w)^T$ and fluxes $F_{IF}(Y) := (0, \rho u, \rho u^2 + p, \phi\rho uv, \phi\rho uw)^T$ (compare [HH2007]: $Y := (\phi, \rho, u, v)$ or $(\phi, \rho, u, \rho u)$). The jump function $\phi(x > 0, y, z, t) := \phi^+ = 0$ vanishes at the '$+$'-side of the interface. Thus the flux F_{IF}^+ satisfies the admissible boundary condition (2.7): $(\phi\rho uv)^+ = 0$, $(\phi\rho uw)^+ = 0$ and the interface model (2.10) is an admissible conservative interface model.

2.3. **Numerical scheme**

We apply the 3D and 1D solver on the 3D resp. 1D domain and use the admissible interface model (2.10) to model the numerical fluxes $F_{IF}^{\pm}$ over the interface. We describe the Riemann problem at the interface in detail. On the 3D or '$-$'-side of the interface we have the left states of the interface Riemann problem defined by

$$Y_{i,j,k}^{3D} := (\phi = 1, \rho, \rho u, \rho v, \rho w)_{i,j,k} = (1, \rho, \rho u, \rho v, \rho w)_{i,j,k} \tag{2.11}$$

for (i, j, k) defined in (1.5) and the 1D or '+'-side we have the right state

$$Y_{i=1}^{1D} := (\phi = 0, \rho, \rho u, \rho v = 0, \rho w = 0)_{i=1} = (0, \rho, \rho u, 0, 0)_{i=1}. \tag{2.12}$$

For the '$-$'-side, we need to compute the numerical fluxes

$$F_{IF}^{-} := F(Y_{i=0,j,k}^{3D}, Y_{i=1}^{1D}, 0^{-})$$

between $Y_{i=0,j,k}^{3D}$ and $Y_{i=1}^{1D}$ for j, k defined in (1.5). As the size of the cross-section (in y and z) at the interface $x_{IF} = 0$ is the same for the '$-$'-side and the '+'-side, the finite volume scheme together with the Green formula give us that F_{IF}^{+} is the sum of all local fluxes $F(Y_{i=0,j,k}^{3D}, Y_{i=1}^{1D}, 0^{+})$ in x- direction by assuming N equally spaced gridcells on the '$-$'-side and one cell on the '+'-side of the interface:

$$F_{IF}^{+} \quad := \sum_{j=0,..,N_y;\ k=0,..N_z} F(Y_{i=0,j,k}^{3D}, Y_{i=1}^{1D}, 0^{+}). \tag{2.13}$$

To receive a consistent numerical 3D-1D coupling method, we use the same finite volume scheme for the cells connected to the interface $x_{IF} = 0$ as in the interior cells of the 3D and 1D domains. But to compute the numerical fluxes $F_{IF}^{\pm}$ at the interface $x_{IF} = 0$, we solve the Riemann problem between the left state $Y^{-} = Y_{i=0,j,k}^{3D}$ and right state $Y^{+} = Y_{i=1}^{1D}$ using (2.10) instead of the two original models (1.1) for the 3D and (1.4) for the 1D part. For the calculation of the numerical fluxes $F_{IF}^{\pm}$ at the interface $x_{IF} = 0$ we consider two Riemann-based schemes: Catum scheme and a Roe-type scheme to solve the Riemann problem between (2.11) and (2.12).

2.3.1. **Catum scheme**

An obvious candidate for the numerical flux calculation is the Riemann-like flux formulation Catum, as used in the interior cells of the 1D and 3D part. The advantage of Catum in comparison with other Riemann-based schemes for the simulation of evolution of cavitation is the uniformly consistency with respect to Mach number. The common used numerical approximation of the cell interface pressure

$$p^{*} = \frac{p_L + p_R}{2} + \frac{\rho_{L,R} c_{L,R} u_{L,R}}{N}$$

is based on compatibility relations and is not uniformly consistent with respect to Mach number. To achieve a uniform consistency in Mach number the numerical fluxes are defined for the admissible conservative interface model (2.10) by

$$F_{IF}^{\pm,Catum} = \rho_L u^{*} \cdot (0, 1, u^{*}, \phi \cdot v_L, \phi \cdot w_L)^{T} + p^{*} \cdot (0, 0, 1, 0, 0)^{T},$$

with the transport velocity u^{*} and the pressure p^{*}

$$u^{*} := \frac{\rho_L c_L u_L + \rho_R c_R u_R + p_L - p_R}{\rho_L c_L + \rho_R c_R}, \quad p^{*} := \frac{p_L + p_R}{2}.$$

To achieve an upwind character for the Catum scheme, the sign of u^{*} is used. The flux $F_{IF}^{\pm,Catum}$ is valid for $u^{*} > 0$. For $u^{*} < 0$ the indices L and R have to be reversed. The basic Catum flux formulation is uniformly

consistent with respect to multidimensional low Mach number flows. For details see [SSST2008]. The Catum scheme has a high numerical dissipation (influence on coupling results see section 2.4), thus as second scheme, a Roe-type scheme, with low dissipation is considered.

2.3.2. **Roe-type scheme**

The interface model (2.10) can be written in condensed form as

$$\partial_t Y + J(Y)\partial_x Y = 0, \tag{2.14}$$

with the matrix $J(Y)$ given by

$$J(Y) = \begin{bmatrix} 0 & 0 & 0 & 0 & 0 \\ 0 & 0 & 1 & 0 & 0 \\ 0 & -u^2+c^2 & 2u & 0 & 0 \\ \rho uv & -\phi uv & \phi v & \phi u & 0 \\ \rho uw & -\phi uw & \phi w & 0 & \phi u \end{bmatrix}$$

and the speed of sound c which verifies

$$c^2 = p'(\rho) > 0. \tag{2.15}$$

For system (2.14) the eigenvalues λ_j, the right-eigenvectors r_j and the normalized left-eigenvectors l_j of the matrix $J(Y)$ (extending the results of [HH2007] by ϕw and use conservative variables) can be analytically calculated by

$$\begin{aligned}
\lambda_1 = 0, \qquad & r_1 = (\phi, 0, 0, -\rho v, -\rho w)^T \\
\lambda_2 = u - c, \qquad & r_2 = (0, -u + c + \phi u, (u-c)(-u+c+\phi u), \phi vc, \phi wc)^T \\
\lambda_3 = \lambda_4 = \phi u, \qquad & \begin{cases} r_3 = (0,0,0,1,0)^T \\ r_4 = (0,0,0,0,1)^T \end{cases} \\
\lambda_5 = u + c, \qquad & r_5 = (0, u + c - \phi u, -(u+c)(-u-c+\phi u), \phi vc, \phi wc)^T \\
\lambda_1 = 0, \qquad & l_1 = \left(\frac{1}{\phi}, 0, 0, 0, 0\right) \\
\lambda_2 = u - c, \qquad & l_2 = \left(0, \frac{-u-c}{-2c^2 - 2c\phi u + 2uc}, \frac{1}{-2c^2 - 2c\phi u + 2uc}, 0, 0\right) \\
\lambda_3 = \lambda_4 = \phi u, \qquad & \begin{cases} l_3 = \left(\frac{\rho v}{\phi}, -\frac{(\phi u^2 - u^2 - c^2)\phi v}{\phi^2 u^2 + u^2 - c^2 - 2\phi u^2}, \frac{\phi uv(\phi - 1)}{\phi^2 u^2 + u^2 - c^2 - 2\phi u^2}, 1, 0\right) \\ l_4 = \left(0, 0, 0, -\frac{w}{v}, 1\right) \end{cases} \\
\lambda_5 = u + c, \qquad & l_5 = \left(0, \frac{c-u}{2c^2 - 2c\phi u + 2uc}, \frac{1}{2c^2 - 2c\phi u + 2uc}, 0, 0\right).
\end{aligned}$$

The first, third and fourth fields are linearly degenerate while the second and the fifth are genuinely non-linear. In comparison with the original Euler equations an additionally stationary wave $\lambda_1 = 0$ at the interface $x_{IF} = 0$ exists for the conservative interface model (2.10).

For a Roe-type scheme, we have to linearize the Riemann problem for (2.14) at the interface $x_{IF} = 0$ between the left Y_L and the right Y_R states.

Definition 3. *For the linearisation of the Riemann problem* (2.14) *we define the vector of averages* $\widehat{Y} := (\widehat{\phi}, \widehat{\rho}, \widehat{\rho u}, \widehat{\rho v}, \widehat{\rho w})^T$. *We recall the original Roe averages* $\widehat{\rho}, \widehat{u}, \widehat{v}, \widehat{w}$*:*

$$\widehat{\rho} = \sqrt{\rho_R \rho_L},\ \widehat{u} = \frac{\sqrt{\rho_R}u_R + \sqrt{\rho_L}u_L}{\sqrt{\rho_R} + \sqrt{\rho_L}},\ \widehat{v} = \frac{\sqrt{\rho_R}v_R + \sqrt{\rho_L}v_L}{\sqrt{\rho_R} + \sqrt{\rho_L}},\ \widehat{w} = \frac{\sqrt{\rho_R}w_R + \sqrt{\rho_L}w_L}{\sqrt{\rho_R} + \sqrt{\rho_L}},$$

and define the averages $\widehat{c}$ *and* $\widehat{\phi}$ *by*

$$\widehat{c} \;=\; \begin{cases} \frac{c_L + c_R}{2} = c_L = c_R & , if\ \triangle\rho = 0, \\ \sqrt{\frac{\triangle p}{\triangle \rho}} & , if\ \triangle\rho \neq 0 \end{cases},$$

$$\widehat{\phi} \;=\; \begin{cases} \frac{1}{2} & , if\ u_L = 0, \\ 1 - \frac{\sqrt{\rho_R}(\sqrt{\rho_R}u_R + \sqrt{\rho_L}u_L)}{u_L(\sqrt{\rho_R} + \sqrt{\rho_L})^2} & , if\ u_L \neq 0\ and\ 0 < \frac{\sqrt{\rho_R}(\sqrt{\rho_R}u_R + \sqrt{\rho_L}u_L)}{u_L(\sqrt{\rho_R} + \sqrt{\rho_L})^2} < 1, \\ 1 & , if\ u_L \neq 0\ and\ \frac{\sqrt{\rho_R}(\sqrt{\rho_R}u_R + \sqrt{\rho_L}u_L)}{u_L(\sqrt{\rho_R} + \sqrt{\rho_L})^2} < 0, \\ 0 & , if\ u_L \neq 0\ and\ \frac{\sqrt{\rho_R}(\sqrt{\rho_R}u_R + \sqrt{\rho_L}u_L)}{u_L(\sqrt{\rho_R} + \sqrt{\rho_L})^2} > 1. \end{cases}$$

We define as initial condition

$$\begin{cases} v_R = w_R = 0, \\ \phi_L = 1,\ \phi_R = 0. \end{cases} \tag{2.16}$$

with ϕ *defined in* (2.9) *and 'L', 'R' defined in Notation 1. Furthermore we define* $\triangle(\cdot) := (\cdot)_R - (\cdot)_L$.

The linearized Riemann problem is defined by

$$\partial_t Y + J(\hat{Y})\partial_x Y = 0, \tag{2.17}$$

with $Y := (\phi, \rho, \rho u, \rho v, \rho w)^T$, the Roe-averages $\widehat{Y} := \left(\widehat{\phi}, \widehat{\rho}, \widehat{\rho u}, \widehat{\rho v}, \widehat{\rho w}\right)^T$ and the initial condition

$$Y(x,0) = \begin{cases} Y_L & , x < 0, \\ Y_R & , x > 0. \end{cases} \tag{2.18}$$

We denote the solution of (2.17)-(2.18) by $Y\left(Y_L, Y_R, \left(\frac{x}{t}\right)^{\pm}\right)$. If we apply a Roe-type scheme for calculating the Riemann fluxes through the coupling interface, we consider the solution at $\frac{x}{t} = 0$:

$$Y\left(Y_L, Y_R, 0^{\pm}\right). \tag{2.19}$$

Proposition 4. *If the linearized Riemann problem* (2.17)-(2.18) *fulfills*

$$\triangle F_{IF}(Y) = \triangle \begin{pmatrix} 0 \\ \rho u \\ \rho u^2 + p \\ \phi \rho u v \\ \phi \rho u w \end{pmatrix} = \triangle\left(J\left(\widehat{Y}\right)Y\right) = J\left(\widehat{Y}\right)\triangle Y \tag{2.20}$$

the difference between the flux on the left F_{IF}^- *and on the right* F_{IF}^+ *side of the interface is exactly preserved.*

Proof. For the second component of $\triangle F_{IF}(Y)$ an easy computation gives $\triangle(\rho u) = \widehat{\rho}\triangle u + \widehat{u}\triangle\rho$.
For the third component, we have to prove

$$\triangle(\rho u^2 + p) = (-\widehat{u}^2 + \widehat{c}^2)\triangle\rho + 2\widehat{u}\triangle(\rho u). \tag{2.21}$$

Using the result for the second component $\triangle(\rho u)$, we obtain

$$\begin{aligned} -\widehat{u}^2\triangle\rho + 2\widehat{u}\triangle(\rho u) &= \widehat{u}(\triangle(\rho u) + \widehat{\rho}\triangle u) \\ &= \widehat{u}((\rho u)_R - (\rho u)_L + \sqrt{\rho_R\rho_L}(u_R - u_L)) \\ &= \widehat{u}(\sqrt{\rho_R}u_R(\sqrt{\rho_R} + \sqrt{\rho_L}) - \sqrt{\rho_L}u_L(\sqrt{\rho_R} + \sqrt{\rho_L})) \\ &= (\sqrt{\rho_R}u_R + \sqrt{\rho_L}u_L)(\sqrt{\rho_R}u_R - \sqrt{\rho_L}u_L) \\ &= \rho_R u_R^2 - \rho_L u_L^2 \\ &= \triangle(\rho u^2). \\ \Rightarrow \quad \triangle(\rho u^2 + p) &= \triangle(\rho u^2) + \widehat{c}^2\triangle\rho. \end{aligned}$$

Finally, equation (2.21) is satisfied

- for $\triangle\rho = 0$, if $\triangle p = 0$. This condition is fulfilled as we use the same equation of state on both sides of the interface and we defined $\widehat{c}$ in Definition 3 as $\widehat{c} := 0.5 * (c_L + c_R) = c_L = c_R$,
- for $\triangle\rho \neq 0$, if $\widehat{c}^2 = \frac{\triangle p}{\triangle\rho}$ holds as given in Definition 3 and using equation (2.15).

For the fourth component of $\triangle F_{IF}(Y)$, the relation

$$\triangle(\phi\rho uv) = \widehat{\rho}\widehat{u}\widehat{v}\triangle\phi - \widehat{\phi}\widehat{u}\widehat{v}\triangle\rho + \widehat{\phi}\widehat{v}\triangle(\rho u) + \widehat{\phi}\widehat{u}\triangle(\rho v), \tag{2.22}$$

has to be verified. We have

$$\begin{aligned} (2.22) \quad &\Leftrightarrow \quad \triangle(\phi\rho uv) - \widehat{\rho}\widehat{u}\widehat{v}\triangle\phi = (-\widehat{u}\widehat{v}\triangle\rho + \widehat{v}\triangle(\rho u) + \widehat{u}\triangle(\rho v))\widehat{\phi} \\ &\Leftrightarrow \quad \triangle(\phi\rho uv) - \widehat{\rho}\widehat{u}\widehat{v}\triangle\phi = (\widehat{u}\widehat{v}\triangle\rho + \widehat{\rho}\widehat{v}\triangle u + \widehat{\rho}\widehat{u}\triangle v)\widehat{\phi}. \end{aligned}$$

If we use the initial condition (2.16), a long (but not difficult) computation gives

$$\begin{cases} \triangle(\phi\rho uv) - \widehat{\rho}\widehat{u}\widehat{v}\triangle\phi = -\rho_L u_L v_L - \frac{\rho_L v_L\sqrt{\rho_R}(\sqrt{\rho_R}u_R + \sqrt{\rho_L}u_L)}{(\sqrt{\rho_R} + \sqrt{\rho_L})^2}\triangle\phi, \\ \widehat{u}\widehat{v}\triangle\rho + \widehat{\rho}\widehat{v}\triangle u + \widehat{\rho}\widehat{u}\triangle v = -\rho_L u_L v_L, \end{cases}$$

and then we obtain

$$(2.22) \quad \Leftrightarrow \quad -\rho_L u_L v_L - \frac{\rho_L v_L\sqrt{\rho_R}(\sqrt{\rho_R}u_R + \sqrt{\rho_L}u_L)}{(\sqrt{\rho_R} + \sqrt{\rho_L})^2}\triangle\phi = -\rho_L u_L v_L\widehat{\phi}.$$

Furthermore, $\widehat{\phi}$ is solution of (2.22), if $\widehat{\phi}$ satisfies

$$-\rho_L u_L - \frac{\rho_L\sqrt{\rho_R}(\sqrt{\rho_R}u_R + \sqrt{\rho_L}u_L)}{(\sqrt{\rho_R} + \sqrt{\rho_L})^2}\triangle\phi = -\rho_L u_L\widehat{\phi}, \tag{2.23}$$

and the fifth equation of $\triangle F_{IF}(Y)$. Replacing v by w the same calculation gives us that $\widehat{\phi}$ has again to fulfill equation (2.23). To fulfill equation (2.23),

- if $u_L = 0$, $\widehat{\phi}$ can be freely chosen and $\widehat{\phi} = \frac{\phi_L + \phi_R}{2} = \frac{1+0}{2} = \frac{1}{2}$, seems evident, even if we know that for $u_R \neq 0$, the relation (2.22) will not be verified.

- if $u_L \neq 0$, we choose $\widehat{\phi} = 1 + \frac{\sqrt{\rho_R}(\sqrt{\rho_R}u_R+\sqrt{\rho_L}u_L)}{u_L(\sqrt{\rho_R}+\sqrt{\rho_L})^2}\triangle\phi$ and the relation (2.20) is satisfied because it yields $\triangle\phi = -1$ at the interface. As defined $\phi \in [0;1]$, it seems natural to choose $\widehat{\phi} \in [0;1]$ and we define:

$$\widehat{\phi} = \begin{cases} 1 - \frac{\sqrt{\rho_R}(\sqrt{\rho_R}u_R+\sqrt{\rho_L}u_L)}{u_L(\sqrt{\rho_R}+\sqrt{\rho_L})^2} & , if\ 0 < \frac{\sqrt{\rho_R}(\sqrt{\rho_R}u_R+\sqrt{\rho_L}u_L)}{u_L(\sqrt{\rho_R}+\sqrt{\rho_L})^2} < 1, \\ 1 & , if\ \frac{\sqrt{\rho_R}(\sqrt{\rho_R}u_R+\sqrt{\rho_L}u_L)}{u_L(\sqrt{\rho_R}+\sqrt{\rho_L})^2} < 0, \\ 0 & , if\ \frac{\sqrt{\rho_R}(\sqrt{\rho_R}u_R+\sqrt{\rho_L}u_L)}{u_L(\sqrt{\rho_R}+\sqrt{\rho_L})^2} > 1. \end{cases}$$

□

Remark 5. *This proof is only valid for the initial condition (2.16) because in this case $\widehat{\phi}$ does not depend on v and w. We recall that if $u_L = 0$ and if $u_R \neq 0$, the relation (2.22) will not be verified and the condition (2.20) is not preserved, but only a small error occurs.*

Solution of the linearized problem. The construction of the solution of the linearized Riemann problem (2.17)-(2.18) is classical, but we briefly recall it for an easy implementation of the Roe-type scheme.
Given the eigenvalues $\lambda_k(\hat{Y})$ with $k = 1, \ldots, 5$ (depicted in Figure 2.3) and the associated right eigenvectors $r_k(\hat{Y})$, we compute β_k such that:

$$Y_R - Y_L = \sum_{k=1}^{5} \beta_k r_k(\hat{Y}).$$

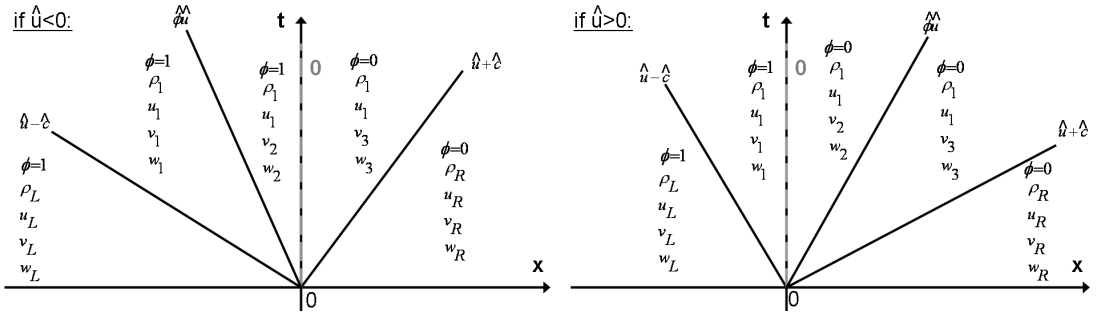

FIGURE 2.3. Characteristics and states of the linearized Riemann problem of the thin interface model considered at the interface with $k = 4 =: L$ and $k = 5 =: R$.

The solution of the linearized Riemann problem (2.17)-(2.18) is given by:

$$Y(x,t) = Y_L + \sum_{\frac{x}{t} < \lambda_l(\widehat{Y})} \beta_l r_l(\widehat{Y}).$$

In order to calculate the solution $Y(x,t)$, we need to compute β_1, β_2 and β_5:

$$\beta_1 = \frac{\phi_R - \phi_L}{\widehat{\phi}}, \quad \beta_2 = \frac{1}{2}\frac{\hat{u}+\widehat{c}}{\widehat{c}(\widehat{c}-\widehat{u}+\widehat{\phi}\widehat{u})}(\rho_R - \rho_L) - \frac{1}{2}\frac{1}{\widehat{c}(\widehat{c}-\widehat{u}+\widehat{\phi}\widehat{u})}((\rho u)_R - (\rho u)_L),$$
$$\beta_5 = \frac{1}{2}\frac{\hat{u}-\widehat{c}}{\widehat{c}(-\widehat{c}-\widehat{u}+\widehat{\phi}\widehat{u})}(\rho_R - \rho_L) - \frac{1}{2}\frac{1}{\widehat{c}(-\widehat{c}-\widehat{u}+\widehat{\phi}\widehat{u})}((\rho u)_R - (\rho u)_L).$$

To compute the solution for all possible values of eigenvectors, we use the left-eigenvectors $l_1(\widehat{Y})$, $l_2(\widehat{Y})$ and $l_5(\widehat{Y})$ because we know that if $\lambda_i \neq \lambda_j$ we have $l_i(\widehat{Y})r_j(\widehat{Y}) = 0$. The solutions $Y(Y_L, Y_R, 0^-), Y(Y_L, Y_R, 0^+)$ at the interface $0^{\pm}$ are then defined by:

- if $\lambda_2(\hat{Y}) > 0$, then $Y(Y_L, Y_R, 0^-) = Y_L$ and $Y(Y_L, Y_R, 0^+) = Y_L + \beta_1 r_1(\widehat{Y})$,
- if $\lambda_2(\hat{Y}) < 0$ and $\lambda_3(\hat{Y}) = \lambda_4(\hat{Y}) > 0$, then $Y(Y_L, Y_R, 0^-) = Y_L + \beta_2 r_2(\hat{Y})$ and $Y(Y_L, Y_R, 0^+) = Y_L + \beta_1 r_1(\hat{Y}) + \beta_2 r_2(\hat{Y})$,
- if $\lambda_3(\hat{Y}) = \lambda_4(\hat{Y}) < 0$ and $\lambda_5(\hat{Y}) > 0$, then $Y(Y_L, Y_R, 0^-) = Y_R - \beta_5 r_5(\hat{Y}) - \beta_1 r_1(\hat{Y})$ and $Y(Y_L, Y_R, 0^+) = Y_R - \beta_5 r_5(\hat{Y})$,
- if $\lambda_5(\hat{Y}) < 0$, then $Y(Y_L, Y_R, 0^-) = Y_R - \beta_1 r_1(\hat{Y})$ and $Y(Y_L, Y_R, 0^+) = Y_R$.

Numerical flux and entropy correction. To compute the numerical flux $F_{IF}(Y(Y_i^n, Y_{i+1}^n, 0^\pm))$, we know the interface states $Y(Y_L^n, Y_R^n, 0^\pm)$ defined in equation (2.19) as solution of the linearized Riemann problem (2.17), we can use the barotropic equation of state $p(\rho, T_0)$ to determine the pressure $p(0^\pm)$ at the interface. The Roe scheme without entropy correction can predict wrong waves and thus authorizes non-physical shocks crossing the interface. It occurs when between two cells Ω_i and Ω_{i+1} an eigenvalue is associated to a non linear k-field: $\lambda_k(Y_L^n) \leq 0 \leq \lambda_k(Y_R^n)$. If and only if a smooth rarefaction wave develops, an entropy correction to guarantee the second principle of thermodynamics is needed. Many numerical entropy corrections exist (e.g. [HH1983]). The approach presented here consists in increasing locally the numerical viscosity of the scheme, as presented in [HHMS2010]. The advantage of this correction is that it is lipschitzian if the numerical flux is lipschitzian.

Definition 6. *(Entropy correction) If $\lambda_k(Y_L^n) \leq 0 \leq \lambda_k(Y_R^n)$ and k-field is non linear, then the numerical flux F_{IF} is replaced by:*

$$F_{IF}(Y(Y_L^n, Y_R^n, 0^\pm)) = F_{IF}(Y(Y_L^n, Y_R^n, 0^\pm)) - \min_k(|\lambda_k(Y_L^n)|, |\lambda_k(Y_R^n)|)\frac{Y_R^n - Y_L^n}{2}.$$

Consequently, with the interface marking function $\phi(x, y, z, t)$ and the admissible coupling boundary condition (2.7), we have a conservative admissible interface model (2.10), which belongs to the thin interface models. Thus the 3D Euler method can be coupled with the 1D Euler method for non-cavitating flows using the interface model (2.10). The details needed for implementing the Catum and Roe-type scheme are given in section 2.4.

Notation 7. *The interface model* (2.10) *belongs to the thin interface models (compare [HH2007]) and is called* ***TI****. Applying the Catum (see section 2.3.1) or the Roe-type scheme (see section 2.3.2) we define the resulting method as* ***TICatum*** *or* ***TIRoe****.*

2.4. Numerical results

The coupling algorithms TICatum and TIRoe for non-cavitating flow passing the interface at $x_{IF} = 0$ are compared to each other and the pure 3D solution calculated by 3D Catum. The domain depicted in Figure 1.1 is decomposed by $\Delta x = \Delta y = \Delta z$ to $N \times N \times N$ equidistant hexahedral gridcells for the pure 3D simulation. For the couplings TICatum or TIRoe the geometry is divided into two parts by locating the interface at $x_{IF} = 0$, the 3D mesh for $x < 0$ with $N_{x,3D} \times N \times N$ and the 1D mesh for $x > 0$ with $N_{x,1D} \times 1 \times 1$ and $N := N_{x,3D} + N_{x,1D}$ number of gridcells. We recall, that for the same cross-section (y- and z-direction) at the interface, there is no jump in geometry at the interface.
As initial condition we assume $p_{init} >> p_{sat}$ and $u = v = w = 0$, with p_{sat} saturation pressure defined by the equation of state and p_{init} the initial pressure. To introduce a pressure wave passing the 3D-1D interface at $x_{IF} = 0$ one or two small regions with a pressure $p_{max} > p_{init}$ are initialised. The corresponding density $\rho(p, T_0)$ is obtained using the barotropic equation of state for a diesel-like test-fluid. All boundaries are assumed as walls. The internal cut of the geometry at $x_{IF} = 0$ for the coupled simulation is modelled by TICatum or TIRoe and the 3D or 1D part is simulated by the 3D or 1D Catum. With this setup, the necessary and sufficient interface coupling condition (2.7): $(\rho uv)^+ = (\rho uw)^+ = 0$ is fulfilled. Both codes use a cfl 1.0 and to assure synchronous timestepping, the minimum of the valid timestep of the 1D and 3D code is used as timestep for both codes.

For the solution of the 3D-1D coupling, we expect that the 3D part of the combined 3D-1D solution yields the same as for the solution for the pure 3D simulation.

Remark 8. *In the following, we only consider the solutions for the x- and y-direction. The results for the z-direction are the same as for the y-direction and are neglected. The results of Figure 2.5 - 2.8 show the solution at the simulation time $t_1 > 0$ or $t_2 > t_1$, corresponding to the time when the wave reaches the interface.*

2.4.1. **Testcase 1: Non-cavitating flow with zero averaged cross-velocities**

By introducing one pressure peak p_{max} as initial condition, we receive a pressure wave, which travels over the interface depending on time t. As depicted in Figure 2.5 at time $t_1 > 0$, the primitive variables are approximated very well by the TIRoe scheme in comparison to the pure 3D solution. The assumption of the constant 1D-values $\rho_{1D}, u_{1D}, p_{1D}(\rho)$ and the cross-velocity $v_{1D} = 0$ as constant right state of the local 3D Riemann problems at the interface $x_{IF} = 0$ for the computation of the fluxes $F^{\pm}_{IF}$ over the interface, implicates small artificial jumps within each local Riemann problem and thus leads to an error in the 3D-1D solution. Especially with the interface model TICatum this error can be detected in the interface connected cells of the 3D part for the velocity u. We achieve a direct comparison of the 1D part solution and the pure 3D solution by averaging the 3D solution with respect to the x-axis. As depicted in Figure 2.6, all results fit very well, with only a small influence in the vicinity of the interface located at $x_{IF} = 0$.

In Figure 2.4 the L^2-errors for the density ρ, the momentum in x-direction ρu and in y-direction ρv calculated with the solver TICatum and TIRoe in comparison with the pure 3D solutions, based on the averaged values depicted in Figure 2.6, are shown. The solutions calculated with the two different flux formulations Catum and Roe are almost the same. Concluding, this testcase illustrates that the interface models TIRoe and TICatum introduce only small errors to the flow in the vicinity of the interface. As shown in the averaged solutions in Figure 2.6, the averaged momentum in y-direction $\rho v = 0$ is zero for the 1D part and thus the solution of $\phi\rho v$ at the interface coincides with the model assumption $(\phi\rho uv)^+ = 0$. A setup with $\rho v \neq 0$ at the interface is considered in the second testcase.

Testcase 1 ($\overline{\mathbf{v}} = 0$)	$\mathbf{L}^2$ – error norm of **Pure 3D – TICatum**	$\mathbf{L}^2$ – error norm of **Pure 3D – TIRoe**
ρ	1.704	1.695
ρ**u**	2151.18	2139.51
ρ**v**	112.03	111.99

Testcase 2 ($\overline{\mathbf{v}} \neq 0$)	$\mathbf{L}^2$ – error norm of **Pure 3D – TICatum**	$\mathbf{L}^2$ – error norm of **Pure 3D – TIRoe**
ρ	0.186	0.191
ρ**u**	168.78	147.13
ρ**v**	173.35	165.26

FIGURE 2.4. L^2-error for the solver TICatum and TIRoe in comparison with the pure 3D solution at time t_1 for testcase 1 (see left side and section 2.4.1) and time $t_2 > t_1$ for testcase 2 (see right side and section 2.4.2).

2.4.2. **Testcase 2: Non-cavitating flow with non-zero averaged cross-velocities**

To achieve a non-zero averaged cross-velocity, two pressure peaks p_{max} are initialised at different x and y locations in the 3D part within the geometry given in Figure 1.1, to obtain an asymmetric cross-velocity field. With this flow field, the strength of influence of the model assumption $(\rho uv)^+ = 0$ of the thin interface model TI can be observed. As shown in Figure 2.7 on the left row, at time $t_1 > 0$ the densities ρ have the same predicates as in the first testcase (see section 2.4.1). To approximate the velocity v in the 1D part, we assume $v_{1D} = 0$. In the right plot of Figure 2.8 we clearly see, that this assumption is fulfilled. The condition $(\rho uv)^+ = 0$ leads to a zero ρv-flux over the interface, thus the momentum in y-direction jumps between the last cell layer of the 3D- and the first cell in the 1D-part. But we also detect an error in the averaged y-momentum at time t_2 for TIRoe and TICatum, which is a result of the jump at the interface. By comparing the L^2-error in the right table of Figure 2.4, the error within the 3D-1D domain is small, which is also depicted on the right three rows in Figure 2.7. Again the TIRoe interface model approximates the solution better than the TICatum model. Thus also for non-zero averaged cross-velocities, the thin interface approach TI seems to be a suitable model for the 3D-1D coupling for the application on non-cavitating flows and especially TIRoe in combination with Catum for the 3D and 1D domain is recommended.

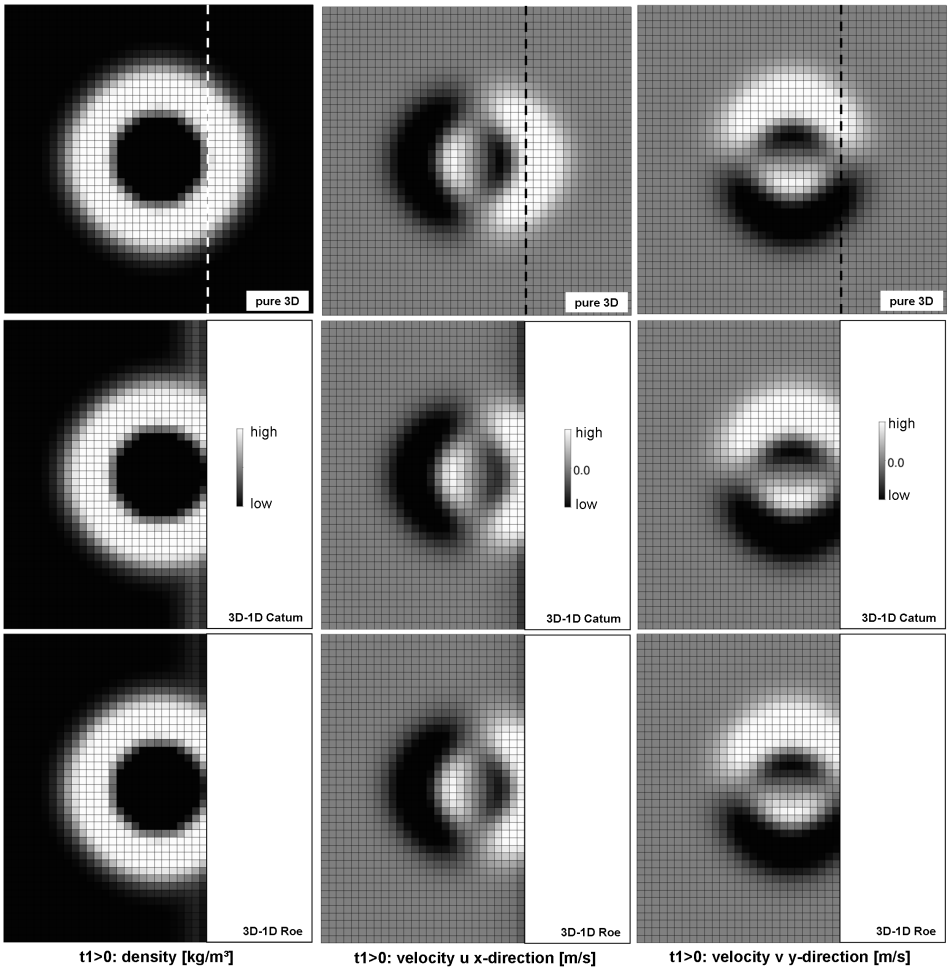

FIGURE 2.5. Non-cavitating testcase with zero average velocities.

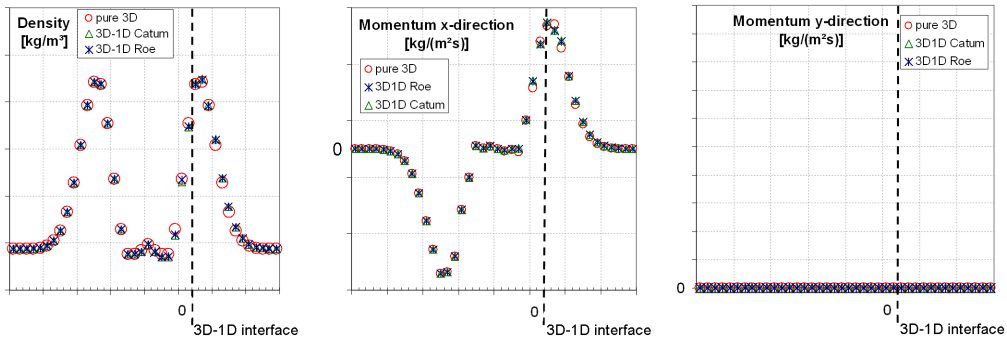

FIGURE 2.6. Averaged solution of the density ρ, momentum in x-direction ρu and momentum in y-direction ρv of the pure 3D, TICatum and TIRoe with respect to the x-axis.

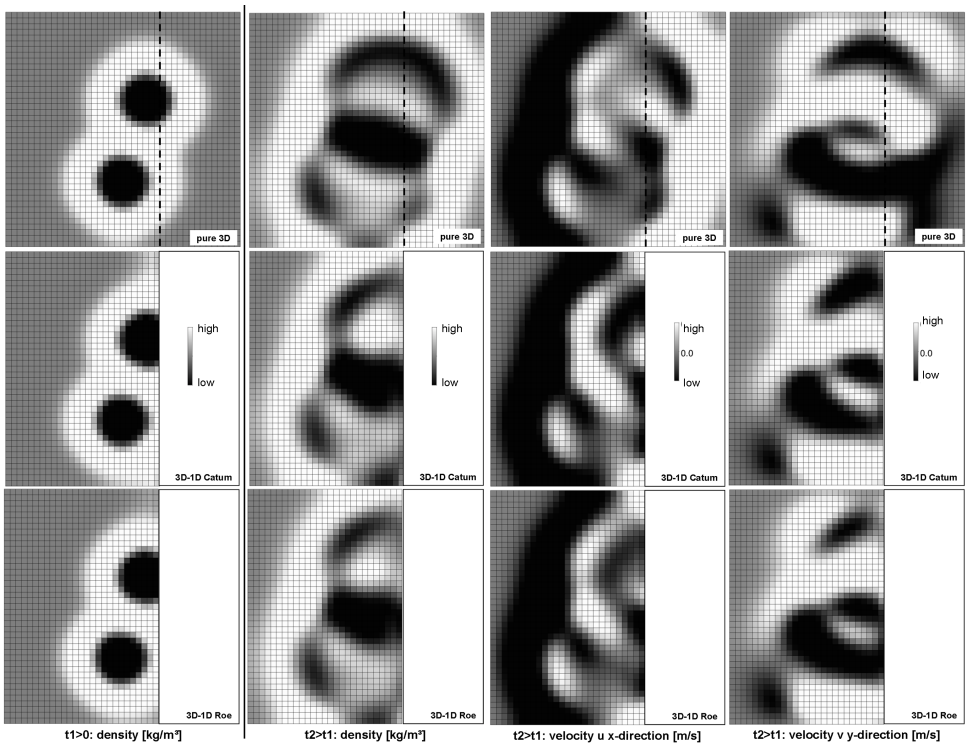

FIGURE 2.7. Non-cavitating testcase with non-zero cross-velocities.

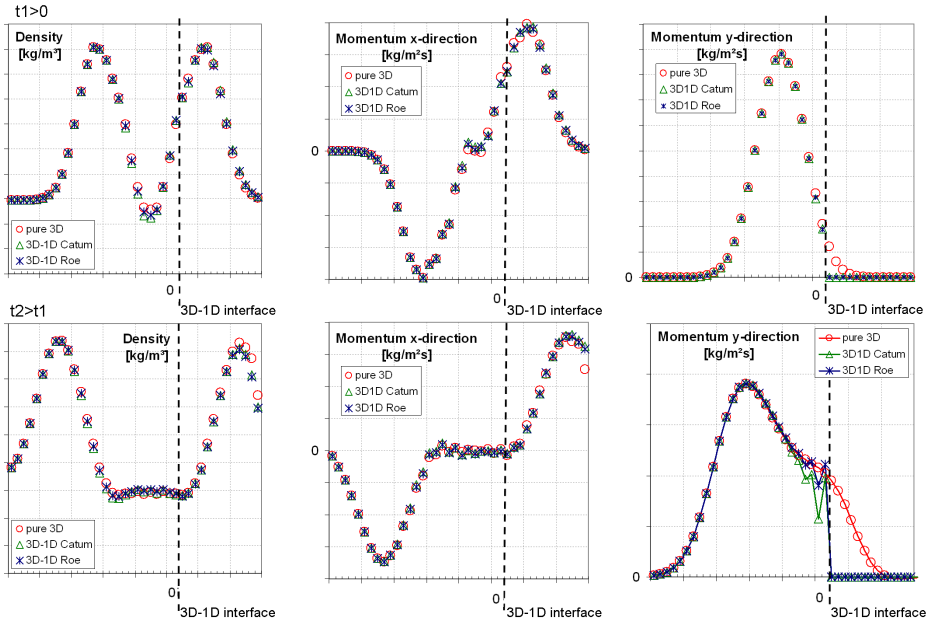

FIGURE 2.8. Non-cavitating testcase with non-zero cross-velocities at time $t_1 > 0$ and $t_2 > t_1$. With respect to the x-axis averaged solutions of density ρ, momentum in x-direction ρu and momentum in y-direction ρv of the pure 3D code, TICatum and TIRoe scheme.

3. Interface model for cavitating flows

Based on the admissible conservative coupling interface model (2.10) for non-cavitating flow passing the interface, an extension to cavitating flow is developed. The limit of interface model (2.10) with respect to cavitating flow passing the interface, is the calculation of the flux for the 1D solver at the interface. An addition of the local three dimensional fluxes is performed (see equation (2.13)), which is not valid for local two-phase regions. The equation of state is non-linear in the two-phase region in comparison with the linear liquid region, which leads to inconsistent densities in the 1D flux for local cavitation regions in the 3D domain at the interface $x_{IF} = 0$. A model considering the local vapor fraction at the interface is needed and developed in this section by splitting the homogeneous density $\rho = \alpha\rho_{liq} + (1-\alpha)\rho_{vap}$ (where α is the volume fraction of liquid) to its liquid ρ_{liq} and vapor ρ_{vap} ratio. Splitting the homogeneous density, the original equation of state is valid over the interface for cavitating flows and cavitation bubbles can pass the interface. We recall that the interface model is only applied for the interface connecting cells. The other fluxes inside the domain are computed by the 3D respectively 1D Catum scheme.

3.1. **Governing equations**

The same barotropic equation of state for a diesel-like test-fluid as mentioned above is used and it is given by a table, which includes the pressure p as function of the homogeneous density ρ, the liquid density $\rho_1 := \rho_{liq}$ and the vapor density $\rho_2 := \rho_{vap}$ and the volume fraction of the liquid phase α with the homogeneous density $\rho = \alpha\rho_1 + (1-\alpha)\rho_2$. This table gives unique pressure laws $p_1 = p_1(\rho_1, T_0)$ and $p_2 = p_2(\rho_2, T_0)$. We are able to consider the ideas described in [CCJK2006] as extension of the interface model (2.10) fulfilling equation (2.7), where the mass conservation is split into two equations coupled by a source term. We define the following interface model:

$$\begin{cases} \partial_t(\tilde{W}) + \partial_x\tilde{F}_{IF}(\tilde{W}) + \partial_y\tilde{G}_{IF}(\tilde{W}) + \partial_z\tilde{H}_{IF}(\tilde{W}) = \tilde{S}_{IF}(\tilde{W}) \\ \partial_t\alpha + u\partial_x\alpha + v\partial_y\alpha + w\partial_z\alpha = k(p_1(\rho_1) - p_2(\rho_2)), \end{cases} \tag{3.1}$$

where

$$\begin{aligned} \tilde{W} &= (\phi, m_1, m_2, \rho u, \rho v, \rho w)^T, \\ \tilde{F}_{IF}(\tilde{W}) &= (0, m_1 u, m_2 u, \rho u^2 + p, \phi\rho uv, \phi\rho uw)^T, \\ \tilde{G}_{IF}(\tilde{W}) &= (0, m_1 v, m_2 v, \rho uv, \rho v^2 + p, \rho vw)^T, \\ \tilde{H}_{IF}(\tilde{W}) &= (0, m_1 w, m_2 w, \rho uw, \rho vw, \rho w^2 + p)^T, \\ \tilde{S}_{IF}(\tilde{W}) &= (0, \lambda(g_2(\rho_2) - g_1(\rho_1)), -\lambda(g_2(\rho_2) - g_1(\rho_1)), 0, 0, 0)^T, \end{aligned}$$

with $\alpha = \frac{V_1}{V_{tot}}$ the volume fraction of the liquid phase, $m_i = \frac{M_i}{V_{tot}}$ (with M_i the mass of phase $i = 1, 2$), $\rho_i = \frac{M_i}{V_i}$ the density of each phase, ϕ is define by (2.9), g_i is the free enthalpy of each phase, that satisfies $\frac{dg_i}{d\rho_i} = \frac{1}{\rho_i}\frac{dp_i}{d\rho_i}$ and the pressure law $p = \alpha p_1(\rho_1) + (1-\alpha)p_2(\rho_2)$.

Remark 9. *If we add the second and the third equations of system (3.1), we obtain* $\partial_t\rho + \partial_x(\rho u) = 0$, *which is the equation of mass conservation. The source terms cancel because of the opposite signs. The last equation of (3.1) can also be written as*

$$\partial_t(\alpha\rho) + \partial_x(\alpha\rho u) + \partial_y(\alpha\rho v) + \partial_z(\alpha\rho w) = k\rho(p_1(\rho_1) - p_2(\rho_2)). \tag{3.2}$$

The splitting of the mass conservation and using a source term, considers the vapor density ρ_2 separately from the liquid density ρ_1. Using this splitting, we can perform a valid addition of fluxes (2.13) at the interface located at $x_{IF} = 0$.

3.1.1. **Properties of model (3.1)**

For smooths solutions $\tilde{Y}$, we can write system (3.1) in condensed form

$$\partial_t \tilde{Y} + J_x(\tilde{Y})\partial_x \tilde{Y} + J_y(\tilde{Y})\partial_y \tilde{Y} + J_z(\tilde{Y})\partial_z \tilde{Y} = \tilde{S}_{IF}(\tilde{Y}), \tag{3.3}$$

where $\tilde{Y} = (\phi, m_1, m_2, \rho u, \rho v, \rho w, \alpha)^T = (\tilde{W}^T, \alpha)^T$, $\tilde{S}_\phi(\tilde{Y}) = (\tilde{S}_{3D}(\tilde{W})^T, k(p_1(\rho_1) - p_2(\rho_2)))^T$ and matrix $J_x(\tilde{Y})$, $J_y(\tilde{Y})$ and $J_z(\tilde{Y})$ are given by

$$J_x(\tilde{Y}) = \begin{bmatrix} 0 & 0 & 0 & 0 & 0 & 0 & 0 \\ 0 & uy_2 & -uy_1 & y_1 & 0 & 0 & 0 \\ 0 & -uy_2 & uy_1 & y_2 & 0 & 0 & 0 \\ 0 & c_1^2 - u^2 & c_2^2 - u^2 & 2u & 0 & 0 & N \\ \rho uv & -\phi uv & -\phi uv & \phi v & \phi u & 0 & 0 \\ \rho uw & -\phi uw & -\phi uw & \phi w & 0 & \phi u & 0 \\ 0 & 0 & 0 & 0 & 0 & 0 & u \end{bmatrix}, \quad J_y(\tilde{Y}) = \begin{bmatrix} 0 & 0 & 0 & 0 & 0 & 0 & 0 \\ 0 & vy_2 & -vy_1 & 0 & y_1 & 0 & 0 \\ 0 & -vy_2 & vy_1 & 0 & y_2 & 0 & 0 \\ 0 & -uv & -uv & v & u & 0 & 0 \\ 0 & c_1^2 - v^2 & c_2^2 - v^2 & 0 & 2v & 0 & N \\ 0 & -vw & -vw & 0 & w & v & 0 \\ 0 & 0 & 0 & 0 & 0 & 0 & v \end{bmatrix},$$

$$J_z(\tilde{Y}) = \begin{bmatrix} 0 & 0 & 0 & 0 & 0 & 0 & 0 \\ 0 & wy_2 & -wy_1 & 0 & 0 & y_1 & 0 \\ 0 & -wy_2 & wy_1 & 0 & 0 & y_2 & 0 \\ 0 & -uw & -uw & w & 0 & u & 0 \\ 0 & -vw & -vw & 0 & w & v & 0 \\ 0 & c_1^2 - w^2 & c_2^2 - w^2 & 0 & 0 & 2w & N \\ 0 & 0 & 0 & 0 & 0 & 0 & w \end{bmatrix},$$

where $y_i = \frac{M_i}{M} = \frac{m_i}{\rho}$, $c_i^2 = \frac{dp_i}{d\rho_i}$ is the squared sound velocity of each phases with $i = 1, 2$ and $N = \frac{\partial p}{\partial \alpha}$. Denoting by c the speed of sound of the mixture, it yields $c^2 = y_1 c_1^2 + y_2 c_2^2$.

To study system (3.3), we have to examine the three matrices $J_x(\tilde{W})$, $J_y(\tilde{W})$ and $J_z(\tilde{W})$. The eigenvalues $\lambda_{x,j=1,..,7}$, right-eigenvectors $r_{x,j=1,..,7}$ and left-eigenvectors $l_{x,j=1,..,7}$ of the matrix $J_x(\tilde{Y})$ are

$$\begin{aligned}
\lambda_{x,1} = 0, \qquad & r_{x,1} = (\phi, 0, 0, 0, -\rho v, -\rho w, 0)^T, \\
& l_{x,1} = (\frac{1}{\phi}, 0, 0, 0, 0, 0, 0), \\
\lambda_{x,2} = u - c, \qquad & r_{x,2} = (0, y_1, y_2, u - c, \frac{\phi v c}{-u + c + \phi u}, \frac{\phi w c}{-u + c + \phi u}, 0)^T, \\
& l_{x,2} = (0, \frac{uc + c_1^2}{2c^2}, \frac{uc + c_2^2}{2c^2}, -\frac{1}{2c}, 0, 0, \frac{N}{2c^2}), \\
\lambda_{x,j=3,4} = u, \qquad & \begin{cases} r_{x,3} = (0, 1, 0, u, 0, 0, -\frac{c_1^2}{N})^T \\ r_{x,4} = (0, 0, 1, u, 0, 0, -\frac{c_2^2}{N})^T \end{cases}, \quad \begin{cases} l_{x,3} = (0, \frac{y_2 c_2^2}{c^2}, -\frac{y_1 c_2^2}{c^2}, 0, 0, 0, -\frac{N y_1}{c^2}) \\ l_{x,4} = (0, -\frac{y_2 c_1^2}{c^2}, \frac{y_1 c_1^2}{c^2}, 0, 0, 0, -\frac{N y_2}{c^2}) \end{cases}, \\
\lambda_{x,j=5,6} = \phi u, \qquad & \begin{cases} r_{x,5} = (0, 0, 0, 0, 1, 0, 0)^T \\ r_{x,6} = (0, 0, 0, 0, 0, 1, 0)^T \end{cases}, \\
& \begin{cases} l_{x,5} = (\frac{\rho v}{\phi}, \frac{(c_1^2 + u^2(1-\phi))\phi v}{u^2 - c^2 + \phi u^2(\phi - 2)}, \frac{(c_2^2 + u^2(1-\phi))\phi v}{u^2 - c^2 + \phi u^2(\phi - 2)}, \frac{uv\phi(1-\phi)}{u^2 - c^2 + \phi u^2(\phi - 2)}, 1, 0, \frac{N\phi v}{u^2 - c^2 + \phi u^2(\phi - 2)}) \\ l_{x,6} = (0, 0, 0, 0, -\frac{w}{v}, 1, 0) \end{cases}, \\
\lambda_{x,7} = u + c, \qquad & r_{x,7} = (0, y_1, y_2, u + c, \frac{\phi v c}{u + c - \phi u}, \frac{\phi w c}{u + c - \phi u}, 0)^T, \\
& l_{x,7} = (0, \frac{c_1^2 - uc}{2c^2}, \frac{c_2^2 - uc}{2c^2}, \frac{1}{2c}, 0, 0, \frac{N}{2c^2}).
\end{aligned}$$

The eigenvalues $\lambda_{y,j=1,..,7}$, right-eigenvectors $r_{y,j=1,..,7}$ and left-eigenvectors $l_{y,j=1,..,7}$ of the matrix $J_y(\tilde{Y})$ are

$$\lambda_{y,1} = 0, \qquad r_{y,1} = (1,0,0,0,0,0,0)^T, \qquad l_{y,1} = (1,0,0,0,0,0,0),$$
$$\lambda_{y,2} = u - c, \quad r_{y,2} = (0, y_1, y_2, u, v-c, w, 0)^T, \quad l_{y,2} = (0, \frac{vc + c_1^2}{2c^2}, \frac{vc + c_2^2}{2c^2}, 0, -\frac{1}{2c}, 0, \frac{N}{2c^2})$$

$$\lambda_{y,j=3,4,5,6} = v, \quad \begin{cases} r_{y,3} = (0,0,0,1,0,0,0)^T \\ r_{y,4} = (0,0,0,0,0,1,0)^T \\ r_{y,5} = (0,1,0,0,v,0,-\frac{c_1^2}{N})^T \\ r_{y,6} = (0,0,1,0,v,0,-\frac{c_2^2}{N})^T \end{cases}, \quad \begin{cases} l_{y,3} = (0,-\frac{uc_1^2}{c^2},-\frac{uc_2^2}{c^2},1,0,0,-\frac{Nu}{c^2}) \\ l_{y,4} = (0,0,0,-\frac{w}{u},0,1,0) \\ l_{y,5} = (0,\frac{y_2c_2^2}{c^2},-\frac{y_1c_2^2}{c^2},0,0,0,-\frac{Ny_1}{c^2}) \\ l_{y,6} = (0,0,0,0,-\frac{w}{v},1,0) \end{cases}$$
$$\lambda_{y,7} = u + c, \quad r_{y,7} = (0, y_1, y_2, u, v+c, w, 0)^T, \quad l_{y,7} = (0, \frac{c_1^2 - vc}{2c^2}, \frac{c_2^2 - vc}{2c^2}, 0, \frac{1}{2c}, 0, \frac{N}{2c^2}),$$

The second and seventh field are genuinely non-linear while others are linearly degenerated.

For eigenvalues $\lambda_{z,j=1,..,7}$, right-eigenvectors $r_{z,j=1,..,7}$ and left-eigenvectors $l_{z,j=1,..,7}$ of the matrix $J_z(\tilde{Y})$ we obtain a similar formula as for matrix $J_y(\tilde{Y})$.

3.2. **Numerical scheme**

To solve system (3.3) with source term $\tilde{S}_{IF}(\tilde{Y})$, we firstly solve the conservative part of (3.3) and secondly, we take the source term into account.

Definition 10. *(M-equilibrium condition) The M-equilibrium condition is fulfilled, if the pressure of the liquid phase p_1 in a gridcell i is the same as the pressure of the vapor phase p_2:*

$$p_1(\rho_1) = p_2(\rho_2). \tag{3.4}$$

The M-equilibrium condition is formally equivalent to suppose $k \to \infty$ in system (3.1) *(see [CCJK2006] for details).*

The M-equilibrium algorithm is subdivided into the following steps.

(1) **Conservative part.** Solve the conservative part of equation (3.3) with a finite volume scheme between time step t_n and t_{n+1}.
   - Update $\tilde{W}$ with a Roe-type scheme and obtain $\tilde{W}^{n+1/2}$.
   - Update α with an upwind scheme (see below) and obtain $\alpha^{n+1/2}$.

   As result receive $\tilde{Y}^{n+1/2} = ((\tilde{W}^{n+1/2})^T, \alpha^{n+1/2})^T$.

(2) **Source term.** Consider the source term $\tilde{S}_{IF}(\tilde{Y})$ with the M-equilibrium condition (3.4). An ordinary differential equation (3.9) has to be solved in $[0; \Delta t]$ with the initial condition $\tilde{Y}^{n+1/2} = \tilde{Y}(x, y, z, 0)$.

(3) **Update α.** Update α such that it satisfies the M-equilibrium (3.4).

3.2.1. **First step: Conservative part**

In this step, we want to solve the conservative part of system (3.3)

$$\begin{cases} \partial_t(\tilde{W}) + \partial_x \tilde{F}_{IF}(\tilde{W}) + \partial_y \tilde{G}_{IF}(\tilde{W}) + \partial_z \tilde{H}_{IF}(\tilde{W}) = 0 \\ \partial_t \alpha + u\partial_x \alpha + v\partial_y \alpha + w\partial_z \alpha = 0, \end{cases} \tag{3.5}$$

with an explicit first order finite volume scheme. The fluxes $\tilde{G}_{IF}$ and $\tilde{H}_{IF}$ are computed with a classical Roe solver (see e.g. [CCJK2006]). The interface flux $\tilde{F}_{IF}$ contains the function ϕ and thus has to be explained. Analog to the Roe linearisation in subsection 2.3, we have to define the state $\hat{\tilde{Y}}$ with $\tilde{Y} = (\tilde{W}^T, \alpha)^T$.

Proposition 11. *The classical Roe averages $\widehat{\rho}$, $\widehat{u}$, $\widehat{v}$ and $\widehat{w}$ are defined as*

$$\widehat{\rho} = \sqrt{\rho_R \rho_L},\ \widehat{u} = \frac{\sqrt{\rho_R}u_R + \sqrt{\rho_L}u_L}{\sqrt{\rho_R} + \sqrt{\rho_L}},\ \widehat{v} = \frac{\sqrt{\rho_R}v_R + \sqrt{\rho_L}v_L}{\sqrt{\rho_R} + \sqrt{\rho_L}},\ \widehat{w} = \frac{\sqrt{\rho_R}w_R + \sqrt{\rho_L}w_L}{\sqrt{\rho_R} + \sqrt{\rho_L}}.$$

Assume $\widehat{y_i}$ as

$$\widehat{y_i} = \frac{\sqrt{\rho_R}y_{i,R} + \sqrt{\rho_L}y_{i,L}}{\sqrt{\rho_R} + \sqrt{\rho_L}}, \quad i = 1, 2$$

and assume that there exists $\widehat{c_i^2}$ and $\widehat{N}$ such that the following discrete jump condition is verified

$$\triangle p = \sum_{i=1,2} \widehat{c_i^2} \triangle(m_i) + \widehat{N} \triangle \alpha.$$

If the initial condition is

$$\begin{cases} v_R = w_R = 0, \\ \phi_L = 1, \quad \phi_R = 0, \end{cases} \tag{3.6}$$

and $\widehat{\phi}$ is defined as

$$\widehat{\phi} = \begin{cases} \frac{1}{2} & , \, if \ u_L = 0 \\ 1 - \frac{\sqrt{\rho_R}(\sqrt{\rho_R}u_R + \sqrt{\rho_L}u_L)}{u_L(\sqrt{\rho_R} + \sqrt{\rho_L})^2} & , \, if \ u_L \neq 0, \end{cases}$$

the relation

$$\begin{pmatrix} \triangle \tilde{F}_{IF}(\tilde{W}) \\ \triangle \alpha \end{pmatrix} = J_x(\widehat{\tilde{Y}}) \triangle \tilde{Y}$$

is satisfied. Thus the difference of the flux on the left F_{IF}^- and on the right F_{IF}^+ side of the interface of system (3.3) *is exactly preserved.*

Proof. The proof is similar to the proof of proposition 4 and thus is not given. □

Remark 12. *As for Proposition 4, the proof is only valid for the initial conditions (3.6) because in this case $\widehat{\phi}$ does not depend on v and w, we recall that if $u_L = 0$ and if $u_R \neq 0$, the jump relation for $\widehat{\phi}$ will not be verified (see Proposition 4).*

To compute the interface flux $\tilde{F}_{IF}$, we have to find the solution $\tilde{Y}(\tilde{Y}_L, \tilde{Y}_R, 0^{\pm})$ of the linearized Riemann problem:

$$\begin{cases} \partial_t \tilde{Y} + J_x(\widehat{\tilde{Y}}) \partial_x(\tilde{Y}) = 0, \\ \tilde{Y}(x, 0) = \begin{cases} \tilde{Y}_L, \, if \ x < 0, \\ \tilde{Y}_R, \, if \ x > 0, \end{cases} \end{cases} \tag{3.7}$$

which is

$$\tilde{Y}(x,t) = \tilde{Y}_L + \sum_{\frac{x}{t} < \lambda_{x,l}(\widehat{\tilde{Y}})} \beta_{x,l} r_{x,l}(\widehat{\tilde{Y}}).$$

To calculate the solution $\tilde{Y}$, we need to identify $\beta_{x,k}$ with $k = 1, 2, 3, 4, 7$, as explained for the eigenvectors of J_x in section 3.1.1:

$$\begin{aligned}
\beta_{x,1} &= \frac{1}{\widehat{\phi}}\triangle\phi \\
\beta_{x,2} &= \frac{\widehat{c_1^2} + \widehat{uc}}{2\widehat{c^2}}\triangle(m_1) + \frac{\widehat{c_2^2} + \widehat{uc}}{2\widehat{c^2}}\triangle(m_2) - \frac{1}{2\widehat{c}}\triangle(\rho u) + \frac{\widehat{N}}{2\widehat{c^2}}\triangle\alpha, \\
\beta_{x,3} &= \frac{\widehat{y_2}\widehat{c_2^2}}{\widehat{c^2}}\triangle(m_1) - \frac{\widehat{y_1}\widehat{c_2^2}}{\widehat{c^2}}\triangle(m_2) - \frac{\widehat{y_1}\widehat{N}}{\widehat{c^2}}\triangle\alpha, \\
\beta_{x,4} &= -\frac{\widehat{y_2}\widehat{c_1^2}}{\widehat{c^2}}\triangle(m_1) + \frac{\widehat{y_1}\widehat{c_1^2}}{\widehat{c^2}}\triangle(m_2) - \frac{\widehat{y_2}\widehat{N}}{\widehat{c^2}}\triangle\alpha, \\
\beta_{x,7} &= \frac{\widehat{c_1^2} - \widehat{uc}}{2\widehat{c^2}}\triangle(m_1) + \frac{\widehat{c_2^2} - \widehat{uc}}{2\widehat{c^2}}\triangle(m_2) + \frac{1}{2\widehat{c}}\triangle(\rho u) + \frac{\widehat{N}}{2\widehat{c^2}}\triangle\alpha.
\end{aligned}$$

The interface states are then defined by

- if $\lambda_{x,2}(\hat{\tilde{Y}}) > 0$, then $\tilde{Y}(\tilde{Y}_L, \tilde{Y}_R, 0^-) = \tilde{Y}_L$ and $\tilde{Y}(\tilde{Y}_L, \tilde{Y}_R, 0^+) = \tilde{Y}_L + \beta_{x,1} r_{x,1}(\widehat{\tilde{Y}})$,
- if $\lambda_{x,2}(\hat{\tilde{Y}}) < 0$ and $\lambda_{x,3}(\hat{\tilde{Y}}) = \lambda_{x,4}(\hat{\tilde{Y}}) > 0$, then $\tilde{Y}(\tilde{Y}_L, \tilde{Y}_R, 0^-) = \tilde{Y}_L + \beta_{x,2} r_{x,2}(\hat{\tilde{Y}})$ and $\tilde{Y}(\tilde{Y}_L, \tilde{Y}_R, 0^+) = \tilde{Y}_L + \beta_{x,1} r_{x,1}(\hat{\tilde{Y}}) + \beta_{x,2} r_{x,2}(\hat{\tilde{Y}})$,
- if $\lambda_{x,3}(\hat{\tilde{Y}}) = \lambda_{x,4}(\hat{\tilde{Y}}) < 0$ and $\lambda_{x,7}(\hat{\tilde{Y}}) > 0$, then $\tilde{Y}(\tilde{Y}_L, \tilde{Y}_R, 0^-) = \tilde{Y}_R - \beta_{x,7} r_{x,7}(\hat{\tilde{Y}}) - \beta_{x,1} r_{x,1}(\hat{\tilde{Y}})$ and $\tilde{Y}(\tilde{Y}_L, \tilde{Y}_R, 0^+) = \tilde{Y}_R - \beta_{x,7} r_{x,7}(\hat{\tilde{Y}})$,
- if $\lambda_{x,5}(\hat{\tilde{Y}}) < 0$, then $\tilde{Y}(\tilde{Y}_L, \tilde{Y}_R, 0^-) = \tilde{Y}_R - \beta_{x,1} r_{x,1}(\hat{\tilde{Y}})$ and $\tilde{Y}(\tilde{Y}_L, \tilde{Y}_R, 0^+) = \tilde{Y}_R$.

Now the three fluxes $\tilde{F}_{3D}$, $\tilde{H}_{3D}$ and $\tilde{G}_{3D}$ can be calculated and we can update $\tilde{W}$. To finish the first step, we have to update α using the second equation of system (3.5) and the following upwind scheme:

$$\alpha_i^{n+1/2} = \alpha_i^n - \frac{\Delta t}{2\Delta x}((\widehat{u}_i^n - |\,\widehat{u}_i^n\,|)(\alpha_{i+1}^n - \alpha_i^n) + (\widehat{u}_i^n + |\,\widehat{u}_i^n\,|)(\alpha_i^n - \alpha_{i-1}^n)). \tag{3.8}$$

3.2.2. **Second step: Source term**

We integrate the ODE system:

$$\begin{cases} \partial_t(\tilde{W}) = \tilde{S}_{IF}(\tilde{W}) \\ \partial_t\alpha = k(p_1(\rho_1) - p_2(\rho_2)), \end{cases} \tag{3.9}$$

over $[0; \triangle t]$ with the initial condition

$$\tilde{Y}(x, y, z, 0) = \tilde{Y}^{n+1/2}(x, y, z, 0).$$

We assume the M-equilibrium (3.4), which means that the last component of the source term $k\rho(p_1(\rho_1) - p_2(\rho_2)) = 0$ is zero or similarly we suppose that α is chosen such that

$$p_1\left(\frac{m_1}{\alpha}\right) = p_2\left(\frac{m_2}{1-\alpha}\right), \tag{3.10}$$

using the pressure laws $p_1(\rho_1, T_0)$ and $p_2(\rho_2, T_0)$. With assumption (3.10), system (3.9) is transferred to

$$\begin{cases} \partial_t(\tilde{W}) = \tilde{S}_{IF}(\tilde{W}) \\ \partial_t\alpha = 0. \end{cases} \tag{3.11}$$

We deduce an approximate ODE system that allows explicit integration instead of a direct numerical integration of system (3.11) to assure stability and maximum principle purpose. Therefore, we scale parameter λ by setting $\lambda = m_1 m_2 \overline{\lambda}$, where $\overline{\lambda}$ is supposed to be a large constant and we fix the $(g_2 - g_1)$ term as $(g_2 - g_1)^{n+1/2}$ evaluated at $\tilde{Y}_i^{n+1/2}$. We obtain the simplified ODE system

$$\partial_t(m_1) = m_1 m_2 \overline{\lambda}(g_2 - g_1)_i^{n+1/2} = m_1(\rho_i^{n+1/2} - m_1)\overline{\lambda}(g_2 - g_1)_i^{n+1/2},\ \partial_t(\rho) = 0,\ \partial_t(\rho u) = 0,$$

which can be solved explicitly

$$m_1(t) = \frac{\rho_i^{n+1/2}}{\left(\frac{\rho_i^{n+1/2}}{(m_1)_i^{n+1/2}} - 1\right) exp\left(-\overline{\lambda} t \rho_i^{n+1/2}(g_2 - g_1)_i^{n+1/2}\right) + 1},\quad \rho(t) = \rho_i^{n+1/2},\quad u(t) = u_i^{n+1/2}.$$

Let us notice that the above relation ensures $m_1(t) \in [0; \rho(t)]$ for all $t > 0$. We now complete the source integration step by setting

$$\rho_i^{n+1} = \rho_i^{n+1/2},\ u_i^{n+1} = u_i^{n+1/2},\ (m_1)_i^{n+1} = m_1(\triangle t),\ (m_2)_i^{n+1} = \rho_i^{n+1} - (m_1)_i^{n+1}.$$

3.2.3. **Third step: Update** α

We update α by remapping α into the M-equilibrium states (3.4). In fact, α^{n+1} is the solution of equation (3.10), then we finally obtain

$$p_1\left(\frac{m_1^{n+1}}{\alpha}\right) = p_2\left(\frac{m_2^{n+1}}{1-\alpha}\right).$$

Remark 13. *The "cavitating" interface model* (3.3) *is not conservative as the admissible conservative interface model* (2.10) *for non-cavitating flows. But the interface model* (3.3) *is valid for cavitating and non-cavitating flow passing the interface. The error received at the interface depends on the amount of cavitation bubbles passing the interface. But this model ensures the same pressure* $p^- = p^+$ *over the interface and changes the volume fraction* α *instead. The constant pressure over the interface is essential for a density-based compressible Euler method and suppress pressure waves introduced by the interface.*

4. Results and Outlook

For the 3D-1D coupling of compressible density-based Euler methods two interface models are evaluated. The first interface model - admissible conservative interface model (2.10) - is valid for non-cavitating and the second interface model (see equation (3.3)) is valid for cavitating and non-cavitating flow passing the coupling interface assumed at $x_{IF} = 0$. The considered domain for the 3D-1D coupling is divided to two parts, a three and a one dimensional domain connected at the coupling interface. Within the 3D part a 3D version of Catum (CAvitation Technical University Munich [SSST2008]) and within the 1D part a 1D version of Catum is used to calculate the (non-) cavitating flow. Only the fluxes over the coupling interface have to be considered by the interface model.

The first "non-cavitating" interface model is based on [HH2007] and uses an interface marking jump function ϕ to perform the jump in dimensions at the coupling interface. For the so called flux coupling approach two Riemann-like flux calculations are considered resulting in two thin interface models TICatum and TIRoe. In section 2.3 all details for an easy implementation of both models are given, which includes the numerical flux formulation for TICatum and the eigenvalues, eigenvectors and Roe averages for the Roe-type interface model TIRoe. As shown in the two testcases in section 2.4.1 and 2.4.2, the thin interface model TICatum and TIRoe perform very well comparing the L^2-error of the averaged solutions and the flow fields. Though our coupling

case is much more complex than the one used in [HH2007], the errors in the vicinity of the interface are small. We recommend as an interface model for non-cavitating flow TIRoe instead of TICatum.

An extension of the interface model (2.10) for non-cavitating to cavitating flow passing the interface is deduced by splitting the density ρ into the vapor density ρ_1 and the liquid density ρ_2 with the homogeneous density $\rho = \alpha\rho_1 + (1-\alpha)\rho_2$. Using two instead of one mass conservation equation, a source and a sink term is modelled using the free enthalpy g_i (see equation (3.1)). Applying the equation of state for the two densities $\rho_i, i = 1, 2$, it is possible to update the volume fraction α. We gain a valid equation of state at the interface for cavitating flows, hence we can add the fluxes at the interface and use them as numerical flux for the 1D code without violating the barotropic equation of state.

Both interface model approaches for non-cavitating and cavitating flow passing the interface can be applied for the 3D-1D coupling of compressible density-based Euler methods for the application on cavitating flow inside the 3D domain. Only for cavitation bubbles passing the interface, the cavitating interface model has to be used. The combination of the ideas of the interface model [HH2007] and the cavitation model given in [CCJK2006] seems to be a sustainable concept for the coupling of three and one-dimensional cavitating flow.

In future works we have to consistently model the local values at the '+'-side for the calculation of local fluxes for the 3D solver at the interface and not only use the constant values given by the 1D solver to reduce the influences of the interface on the flow in the vicinity of the interface as depicted in section 2.4. Overall the two proposed interface models (2.10) and (3.3) for the coupling of 3D and 1D Euler methods have a high potential for considering an entire (non-) cavitating hydraulic system behaviour and also with acceptable computational costs in comparison with a pure 3D simulation for the entire hydraulic system.

5. Acknowledgments

This work was supported by Robert Bosch GmbH. It has benefited amongst others from fruitful discussions with Jean-Marc Hérard (Électricité de France R & D) and Frédéric Coquel (DR CNRS at CMAP, École Polytechnique, Palaiseau) during CEMRACS 2011.

References

[BGH2000] T. Buffard, T. Gallouet, J-M. Hérard. A sequel to a rough Godunov scheme. Application to real gases. Computers & Fluids, 29, pp: 813-847, 2000.

[CCJK2006] F. Caro, F. Coquel, D. Jamet, S. Kokh. A simple finite-volume method for compressible isothermal two phase flows simulation. International Journal on Finite Volume Vol. 3, no. 1, pp: 7, 2006. http://www.latp.univ-mrs.fr/IJFV/

[G1959] S.K. Godunov (1959). A Difference Scheme for Numerical Solution of Discontinuous Solution of Hydrodynamic Equations. Math. Sbornik, 47, pp: 271-306, translated US Joint Publ. Res. Service, JPRS 7226, 1969.

[GR1996] J. M. Greenberg, A. Y. Le Roux. A well balanced scheme for the numerical processing of source terms in hyperbolic equation. SIAM J Numer Anal 1996; 33 (1) pp: 1-16.

[HH1983] A. Harten, J. Hyman. Self-adjusting grid methods for one dimensional hyperbolic conservation laws. J. Comput. Phys., 50(2), pp. 235-269, 1983.

[HH2007] J.-M. Hérard, O. Hurisse. Coupling two and one-dimensional unsteady Euler equations through a thin interface. Computers and fluids, 36 (2007) 651-666.

[HHMS2010] P. Helluy, J.-M Hérard, H. Mathis, S. Müller. A simple parameter-free entropy correction for approximate Riemann solvers. Comptes rendus Mécanique, Vol. 338, Issue 9, pp. 493-498, 2010.

[NII2011] M. Nohmi, T. Ikohagi, Y. Iga. On boundary conditions for cavitation CFD and system dynamics of closed loop channel. Proceedings of the ASME-JSME-KSME 2011 Joint Fluids Engineering Conference AJK-Fluids2011, AJK2011-33007.

[SIMMSA2011] R. Skoda, U. Iben, A. Morozov, M. Mihatsch, S. J. Schmidt, N. A. Adams. Numerical simulation of collapse induced shock dynamics for the prediction of the geometry, pressure and temperature impact on the cavitation erosion in micro channels. Warwick WIMRC 3rd International Cavitation Forum 2011.

[SSST2008] S. J. Schmidt, I. H. Sezal, G. H. Schnerr, M. Talhamer. Riemann Techniques for the Simulation of Compressible Liquid Flows with Phase-transition at all Mach numbers - Shock and Wave Dynamics in Cavitating 3-D Micro and Macro Systems. AIAA paper 2008-1238.